The Double-Peaked El Niño and Its Physical Processes

NA-YEON SHIN,[a] JONG-SEONG KUG,[a] F. S. MCCORMACK,[b] AND NEIL J. HOLBROOK[c,d]

[a] *Division of Environmental Science and Engineering, Pohang University of Science and Technology, Pohang, South Korea*
[b] *School of Earth, Atmosphere and Environment, Monash University, Clayton, Victoria, Australia*
[c] *Institute for Marine and Antarctic Studies, University of Tasmania, Hobart, Tasmania, Australia*
[d] *ARC Centre of Excellence for Climate Extremes, University of Tasmania, Hobart, Tasmania, Australia*

(Manuscript received 3 June 2020, in final form 9 November 2020)

ABSTRACT: Recently, El Niño diversity has been paid much attention because of its different global impacts. However, most studies have focused on a single warm peak in sea surface temperature anomalies (SSTAs), either in the central Pacific or the eastern Pacific Ocean. Here, we demonstrate from observational analyses that several recent El Niño events show double warm peaks in SSTA—called ''double-peaked (DP) El Niño''—that have only been observed since 2000. The DP El Niño has two warm centers, which grow concurrently but separately, in both the central and eastern Pacific. In general, the atmospheric and oceanic patterns of the DP El Niño are similar to those of the warm-pool (WP) El Niño from the development phase, such that the central Pacific peak is developed by the zonal advective feedback and reduced wind speed anomalies. However, a distinctive difference exists in the eastern Pacific where the DP El Niño has a second SSTA peak. In addition, the DP El Niño shows more distinctive anomalous precipitation along the Pacific intertropical convergence zone (ITCZ) when compared with the WP El Niño. We demonstrate that the peculiar precipitation anomalies along the Pacific ITCZ play a critical role in enhancing the equatorial westerly wind stress anomalies, which help to develop the eastern SSTA peak by deepening the thermocline in the eastern Pacific.

KEYWORDSS: Ocean dynamics; El Niño; Air–sea interaction, Heat budgets/fluxes

1. Introduction

Over the past several decades, our understanding of the El Niño–Southern Oscillation (ENSO) phenomenon has increased substantially (Bjerknes 1969; Wyrtki 1975; Rasmusson and Carpenter 1982; Philander et al. 1984; Cane and Zebiak 1985; Jin 1997a,b; Timmermann et al. 2018; Cai et al. 2019). A recent focus has been on ENSO spatial diversity because the different patterns of sea surface temperature anomalies (SSTA) can influence the atmospheric convection, which leads to different global impacts on the distribution of precipitation, temperature, and atmospheric pressure (Hoerling et al. 1997; Trenberth et al. 1998; Capotondi et al. 2015). The classic categorization is that there are two distinct types of El Niño, and there are various terms to refer to this. The canonical El Niño, having SSTA maximum in the eastern Pacific Ocean, is called the cold-tongue (CT) El Niño or the eastern Pacific El Niño. The other type of El Niño, having a SSTA maximum in the central Pacific, is called the warm-pool (WP) El Niño, the central Pacific El Niño, the El Niño Modoki, or the date line El Niño (Larkin and Harrison 2005a,b; Ashok et al. 2007; Kug et al. 2009; Kao and Yu 2009).

Kug et al. (2009) showed that the WP and CT El Niños have different dynamical mechanisms of their development and decay phases. For example, the CT El Niño is mostly developed by the thermocline feedback. In general, the CT El Niño has stronger westerly wind anomalies, and the center of maximum heating is shifted eastward of that of the WP El Niño, which leads to a clear seesaw pattern in the equatorial thermocline. The deepened thermocline in the eastern Pacific easily induces sea surface warming in the eastern Pacific, which is a major process for the development of CT El Niño. However, the magnitude of the westerly wind anomalies associated with the WP El Niño is relatively weak and shifted westward, so that it hardly deepens the eastern Pacific thermocline. Instead, the eastward currents, due to both geostrophic and wind-driven currents, are evident in the central Pacific during its development phase, which accompanies considerable warm advection where the climatological zonal temperature gradient is strong. In addition, the westerly anomaly reduces the trade winds, which can help to develop surface warming by reducing evaporation. This is more effective where the climatological SST is high. These different mechanisms of the two El Niño types lead to their different location of SSTA that could induce different global impacts (Kug et al. 2010a; Shi et al. 2019; Capotondi et al. 2019).

In a recent analysis of the representation of ENSO in 36 CMIP5 coupled model simulations, a peculiar pattern of El Niño was recognized by Graham et al. (2017): the double-peaked (DP) El Niño. In the DP El Niño, the two warm centers are separated, growing simultaneously in both the eastern and central Pacific. They argued that the DP El Niño is an issue seen only in coupled climate model simulations, and its existence is due to the models' cold-tongue bias in the equatorial central and eastern Pacific. By analyzing the mean location of the dynamic warm-pool edge (DWPE; i.e., the maximum zonal salinity gradient), they showed that the central Pacific warm

Supplemental information related to this paper is available at the Journals Online website: https://doi.org/10.1175/JCLI-D-20-0402.s1.

Corresponding author: Jong-Seong Kug, jskug1@gmail.com

DOI: 10.1175/JCLI-D-20-0402.1

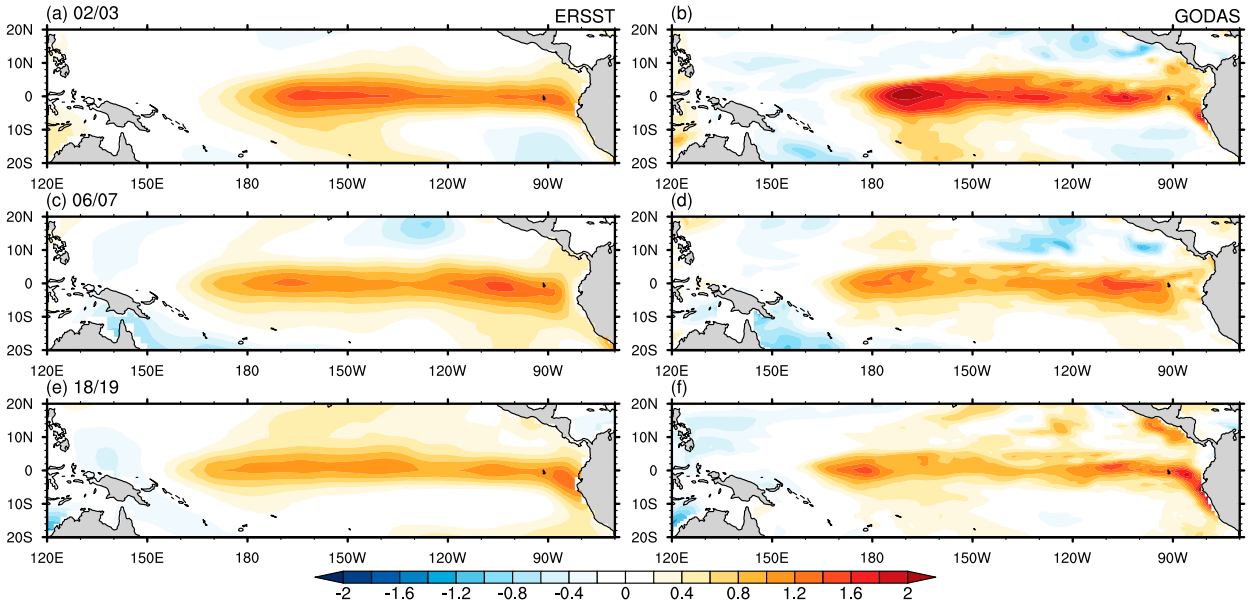

FIG. 1. Individual SSTA pattern (°C) of NDJ for each DP El Niño event [(a),(b) 2002/03; (c),(d) 2006/07; and (e),(f) 2018/19] (left) from ERSST and (right) from GODAS.

peak is related to the magnitude of the cold-tongue bias, as manifested by its unrealistic westward displacement (Brown et al. 2013). They also pointed out that the DP El Niño emerges more frequently in the preindustrial *PiControl* coupled CMIP simulations, because they display a stronger cold tongue due to the lower CO_2 concentrations, relative to results from *historical* simulations, which include the effects of historical increases in atmospheric CO_2.

As the DWPE moves toward the western Pacific because of the cold-tongue bias, the westerly wind anomalies and resultant eastward current anomalies occur farther westward. Also, the maximum of the climatological zonal temperature gradient moves westward (Picaut et al. 1996, 1997; Clarke et al. 2000). Thus, the zonal advective feedback term, by the eastward current anomalies and climatological zonal temperature gradients, leads to the warm center in the central Pacific. Additionally, the net surface heat flux contributes to the development of the central peak since the cold-tongue bias reduces the cloudiness, leading to an increase in incoming shortwave radiation due to the weak SST–cloud interaction (Rashid and Hirst 2015). The eastern SSTA warm peak of the DP El Niño is generated by the thermocline feedback term, climatological upwelling, and anomalous vertical temperature gradients. However, the magnitude of this peak is weaker than for the CT El Niño because the westerly wind stress anomalies of the DP El Niño are located farther west.

Interestingly, Graham et al. (2017) argued that DP El Niños are not found in the historical observational data because of the absence of a cold-tongue bias in the real world. In the present study, with the analysis of longer observational records from 1980 to 2018, we were able to identify at least three characteristic DP El Niño events. This study not only aims to detect DP El Niño events in the observational record but also aims to identify the characteristic drivers and mechanisms of these events. The individual SSTA pattern of each DP El Niño is shown in Fig. 1. While there is overall warming in the eastern and central Pacific, the warm centers are clearly separated. The location of the central or eastern peak is very similar to the respective location of the WP or CT El Niño center. Since the SSTA peaks are separated, any conventional ENSO indices such as Niño-3, Niño-3.4, and Niño-4 SSTA cannot identify both peaks. In this study, we examined characteristics of this new type of El Niño and suggest a possible mechanism. We briefly discuss the data and methods in section 2. Section 3 explains how each peak develops separately. Last, a summary and discussion are given in section 4.

2. Data and methods

a. Observational data

We use the NOAA Extended Reconstructed Sea Surface Temperature (ERSST), version 5 (Huang et al. 2017), with $2° \times 2°$ resolution as the primary data analyzed in this study to detect the DP El Niño in the observations. We use monthly mean zonal wind stress, oceanic currents, sea surface height, and vertical potential temperature obtained from Global Ocean Data Assimilation System (GODAS) with $0.333° \times 1.0°$ resolution (Behringer and Xue 2004). The potential temperature and currents are used for the heat budget analysis (Huang et al. 2010). The monthly mean precipitation data are from the CPC Merged Analysis of Precipitation (CMAP) with $2.5° \times 2.5°$ resolution (Xie and Arkin 1997). Last, the monthly mean wind speed data at sigma level 0.955 (from the daily wind speed) and zonal wind at 850 hPa are from the National

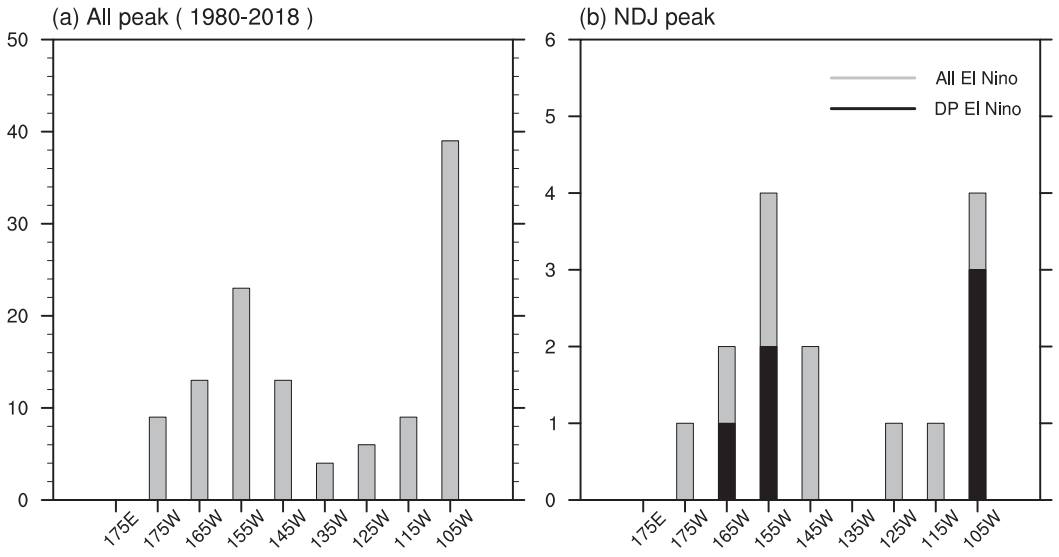

FIG. 2. The longitudinal structure of the SST peaks. The peaks are counted from (a) all months and (b) only NDJ. Gray bars represent the single peak, and black bars represent the double peaks. The *x* axis is longitude; the *y* axis is the number of peaks.

Centers for Environmental Prediction–National Center for Atmospheric Research (NCEP–NCAR) reanalysis 1 with 2.5° × 2.5° resolution (Kalnay et al. 1996). All of these data sources cover the period from January 1980 to February 2019.

b. Methods

As outlined in the introduction, this study aims to first detect DP El Niño events in the 40-yr observational record of ERSST data, and second to identify the developing mechanisms of these events. However, before we define what a DP El Niño is, we first develop an algorithm to detect local maximum SSTA because typically used area-averaged ENSO indices are unable to detect DP El Niños. First, we carry out a 3-month running mean SSTA and removed the long-term trend. Second, we averaged the data meridionally (from 2°S to 2°N) and calculated a moving average with a 30° longitude window from 160°E to 90°W. The window is progressively moved by a 10° interval (from 160°E–170°W to 120°–90°W; nine points). Third, if the moving SSTA is greater than 1 standard deviation of the SSTA, we define it as a warm point. If at least one warm point is detected during November–January (NDJ) of a certain year, that year is defined as an El Niño year. On the basis of this criterion, a total of 12 El Niño events are detected from 1980 to 2018.

Next, to separate El Niño types based on the longitudinal SSTA distribution, we try to identify a local maximum in the SSTA. If a warm point is isolated, it is selected as a local peak. Otherwise, if the warm points are adjacent, we detected the local peaks among the consecutive warm points. If there is a single local peak in NDJ, the case is classified as either a WP or CT El Niño depending on the longitude of the warm center. If there is a double peak in NDJ, the case is classified as a DP El Niño.

Figure 2 shows the longitudinal distribution of the number of local SSTA peaks. For all months (Fig. 2a), it is evident that the number distribution shows a clear bimodal structure. One center is located in the central Pacific, and the other is near the eastern boundary of the equatorial Pacific. That is, the highest frequency of the local peaks occurs at 155° and 105°W. In addition, there are only two cases that have their SSTA maxima at 135°W as shown in Fig. 2a.

When we only consider the ENSO peak time (NDJ), the distribution still shows a bimodal structure (Fig. 2b), with no cases of SSTA maximum at 135°W. The bimodal structure suggests the possibility that at least two distinct physical modes exist in the tropical Pacific, which can explain the zonal diversity of the ENSO patterns. Due to the clear separation, we easily classify the WP El Niño and CT El Niño based on the location of their SSTA peaks with the 135°W criterion. In other words, if the peak is located to the west of 135°W, the event is defined as WP El Niño; if the peak is to the east of 135°W, it is defined as CT El Niño.

Interestingly, of the 12 El Niño events in the record, nine events show a single peak, but three events (2002/03, 2006/07, 2018/19) have two local peaks. In this study, these three El Niño events are classified as DP El Niño, and the others are classified as WP (1986/87, 1987/88, 1991/92, 1994/95, 2004/05, 2009/10) or CT El Niños (1982/83, 1997/98, 2015/16) depending on the location of the SSTA peak.

c. The mixed layer heat budget

To understand the dynamical processes that underpin the development of the SSTA, we analyzed the mixed layer temperature (MLT) tendency budget. Because the two warm centers evolve separately, we examine each center respectively. We use MLT to examine the heat budget as we checked

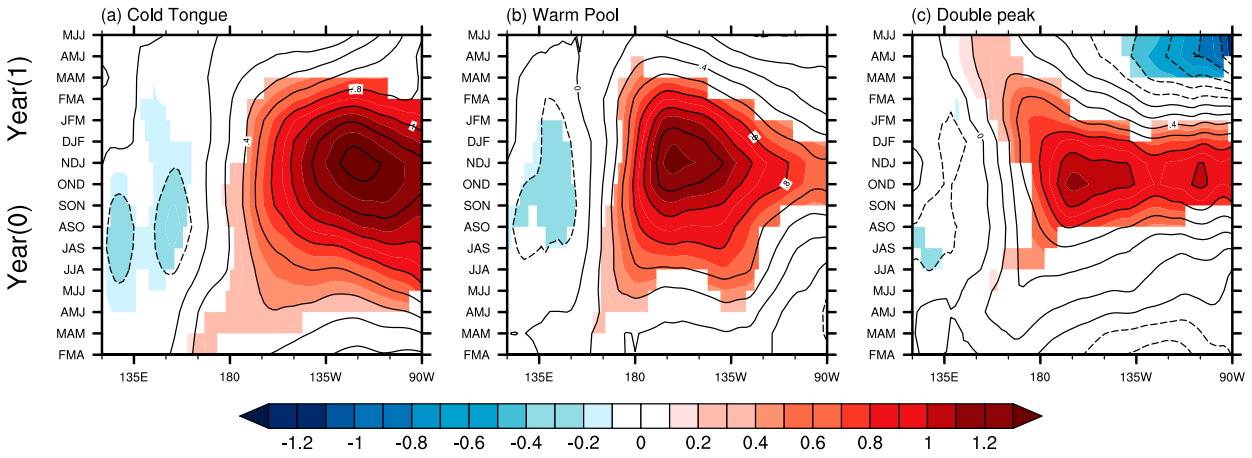

FIG. 3. Composite evolution of (a) the CT El Niño SSTA, (b) the WP El Niño SSTA, and (c) the DP El Niño SSTA. The SSTA is normalized by the NDJ SSTA index of each year and so is unitless. The *x* axis is longitude, and the *y* axis is months of the year of El Niño–type evolution. Shadings indicate the 90% confidence level as based on a two-tailed one-sample *t* test.

the consistency of MLT and SST (not shown). The equation for the temperature tendency budget is as follows:

$$\frac{\partial T'}{\partial t} = -u'\frac{\partial \overline{T}}{\partial x} - v'\frac{\partial \overline{T}}{\partial y} - w'\frac{\partial \overline{T}}{\partial z} - \overline{u}\frac{\partial T'}{\partial x} - \overline{v}\frac{\partial T'}{\partial y} - \overline{w}\frac{\partial T'}{\partial z} - u'\frac{\partial T'}{\partial x} - v'\frac{\partial T'}{\partial y} - w'\frac{\partial T'}{\partial z} + R,$$

where overbars and primes are monthly climatology and anomaly, respectively; u, v, and w indicate the zonal, meridional, and vertical oceanic current velocity components; T is MLT; and t is time. For the temperature budget analysis, a fixed mixed layer depth (50 m) is assumed, but the main results from the heat budget analysis are not sensitive to the definition of the mixed layer depth (not shown). The w term is calculated at the bottom of the mixed layer and other values are averaged over the mixed layer. The term R represents the residual processes. Derivatives are calculated by the centered difference method. This method of budget analysis is similar to (Kang et al. 2001). To focus on the SSTA development through to the mature phase, the temperature tendency budget is averaged from August to November in the El Niño development year.

d. Linear baroclinic model

In section 3, a linear baroclinic model (LBM) experiment is conducted to confirm the atmospheric response to the diabatic heating forcing. The LBM is a linear baroclinic model of atmosphere and it is based on the linear governing equation about a basic state [see Watanabe and Kimoto (2000) for the detailed mathematical expressions]. The prescribed heating is obtained from the observed precipitation pattern of the WP and DP El Niño by assuming a vertical structure, having a maximum at the $\sigma = 0.45$ level. This model has a resolution of T21 and with 20 vertical levels (T21 L20) and the time is integrated 30 days to obtain the quasi-steady state. The basic state is monthly climatology from 1980 to 2018. The experimental design is similar to previous studies (Son et al. 2014; Kim et al. 2018).

3. Results

a. Distinct El Niño patterns

Figure 3 shows the evolution of SSTA for the WP, CT, and DP El Niños. To emphasize the pattern differences, the SSTA is normalized by dividing by the NDJ SSTA of each year averaged over the central to eastern Pacific (160°E–90°W). The warm center of the CT El Niño is located in the eastern Pacific and the center of the WP El Niño is located in the central Pacific, by definition. The DP El Niño has two warm centers in both the eastern Pacific and central Pacific. Note that the central peak of the DP El Niño is located in a similar region to the WP El Niño, but the eastern peak is located to the east of the CT El Niño's peak. The DP El Niño tends to develop later and to decay earlier so that the duration is shorter than either of the other El Niño types. Strictly speaking, the central Pacific SSTA slowly evolves and develops with an eastward propagation in the development year, and slowly decays with a westward propagation in the decaying year. However, the eastern Pacific SSTA rapidly develops and decays. For example, the sign of the eastern Pacific SSTA changed to positive in the MJJ and then changed to negative in the next FMA. These distinct evolutions of the central and eastern Pacific SSTA suggest that different dynamical processes operate for the two centers. Also, we found that the seasonal phase locking to the early winter is consistent across the three El Niños as shown in Fig. 3.

Figure 4 shows the atmospheric and oceanic patterns during the mature phase (NDJ) of each El Niño type. As expected, each type shows a distinct SSTA pattern. The DP El Niño is narrower in meridional SSTA width than the others. Atmospheric variables also show different spatial patterns for the three types of El Niño. The different patterns and locations

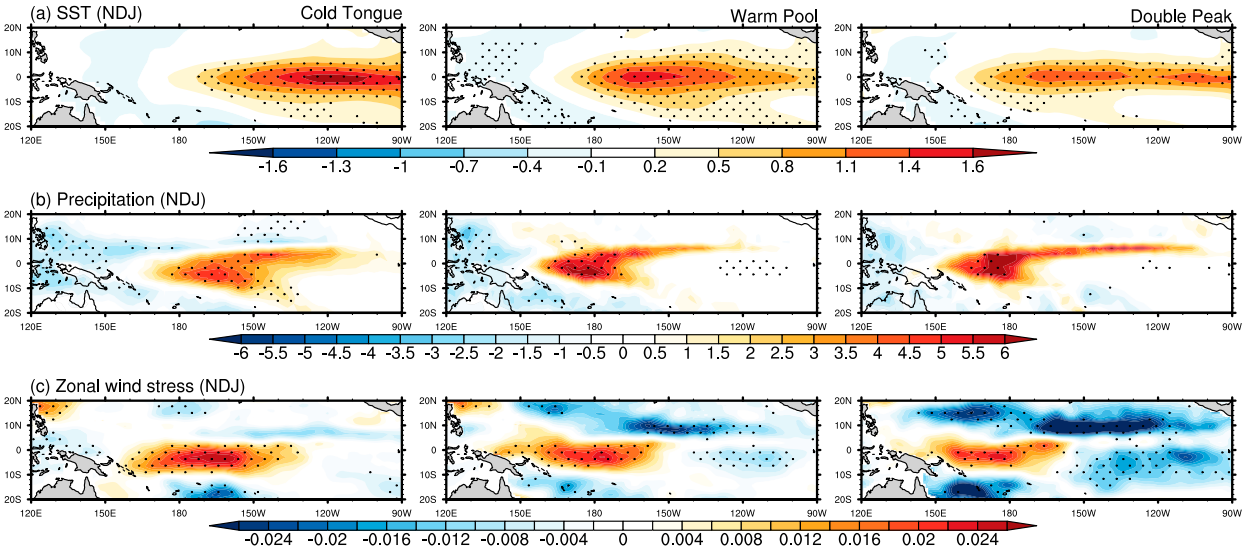

FIG. 4. Composites of the mature phase (NDJ) of (a) SST anomalies (unitless), (b) precipitation anomalies (mm day^{-1} °C^{-1}), and (c) zonal wind stress anomalies (N m^{-2} °C^{-1}) (all variables are normalized as in Fig. 3) for (left) the CT El Niño, (center) the WP El Niño, and (right) the DP El Niño. Stippling indicates the 90% confidence level.

between the CT El Niño and WP El Niño have been previously reported (e.g., Kug et al. 2009). The anomalous precipitation and zonal wind stress patterns for the CT El Niño are shifted eastward relative to the others. The central peak of the DP El Niño shows a very similar zonal location to that of the WP El Niño. For these two types of El Niño, the pattern of equatorial westerly wind stress anomalies is similar in the western and central Pacific. Interestingly, the easterly wind stress anomalies are stronger in the eastern Pacific for the DP El Niño despite the warmer eastern Pacific SSTA. While the overall anomalous precipitation patterns are similar between the DP and WP El Niño types, a distinctive difference is found at latitudes that are off the equator. The DP El Niño shows a strong and concentrated positive precipitation anomaly along the Pacific ITCZ over the central and eastern Pacific, which may play a role in El Niño development. In the next section, we examine the different dynamical processes that evolve in the WP and DP El Niño.

b. *The central peak of the DP El Niño*

We first examine the central peak of the DP El Niño compared with the WP El Niño. Figure 5a shows each term of the WP and DP El Niños for the central peak (175°–145°W), where many maximum peaks exist as shown in Fig. 2b. It is shown that the zonal advective feedback term by the anomalous currents and climatological temperature gradient is the dominant term in the central peak of the DP El Niño in Fig. 5a. The climatological SST gradient is westward, so the anomalous eastward currents induce surface warming. The anomalous eastward current can be generated by geostrophic and wind-driven currents. The DP El Niño has maximum sea level anomalies at the equator meridionally. Thus, those anomalous sea level patterns lead to the anomalous geostrophic eastward currents (Hirst 1986; Wang and Weisberg 1994; Su et al. 2010) as well as the westerly induced eastward current anomalies. Also, the meridional advection by the climatological divergent currents is large for both El Niños (Figs. 5a,b), related to the poleward expansion of the equatorial SSTA (Kang et al. 2001), so that it does not have an active role in developing but it is a consequence of the warm center. In addition, the meridional advection by the anomalous currents is positive for both El Niño events in Fig. 5a, possibly due to the Ekman convergence by the westerly anomaly, but its magnitude is relatively weak.

Interestingly, this zonal advective term is relatively weak for the WP El Niño. Previous studies argued that the zonal advective feedback term is also dominant in the WP El Niño (Kug et al. 2010b), which is inconsistent with our results. However, we found that the relatively weak zonal advective term in the WP El Niño is related to the timing of the SSTA development. As shown in Fig. 6a, the zonal advective term of the WP El Niño stays positive during the development phase, but its magnitude is stronger in late spring and early summer, and gradually weakens afterward. However, the evolution of the DP El Niño is very different. The zonal advective feedback of the DP El Niño is weakly positive in the early summer but rapidly increases to a much larger peak than for the WP El Niño in late summer and early autumn (Fig. 6a). In other words, the zonal advective term is dominant for both WP and DP El Niño, but its evolution differs for each. The thermocline feedback term of the WP El Niño is relatively large in the spring season, but it gradually weakens in Fig. 6b. The DP El Niño also shows a positive contribution of the thermocline feedback term, but it is relatively weaker than the zonal advective term in Fig. 6a.

In addition to the zonal advective feedback, the latent heat flux can be also important for the central SSTA for the WP El Niño (Kug et al. 2010b). Due to the lack of an accurate heat flux observation, we use the anomalous wind speed along the equator as a proxy, as shown in Fig. 7. Near the date line,

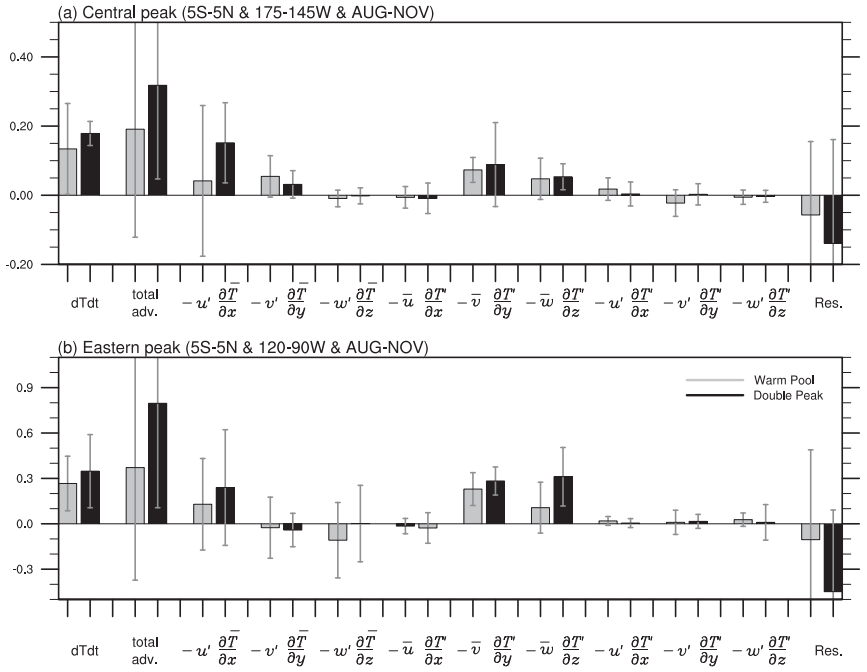

FIG. 5. Normalized temperature tendency (month^{-1}) budget analysis of (a) the central peak area (5°S–5°N, 175°–145°W) and (b) the eastern peak area (5°S–5°N, 120°–90°W). Gray bars represent the WP El Niño, and black bars represent the DP El Niño. The error bars indicate the 90% confidence level.

negative wind speed anomalies exist in both the WP and DP El Niños. The reduced wind speed anomaly is related to the westerly anomaly there under the climatological easterly wind. The reduced wind speed anomaly is conducive to less evaporation, which leads to surface warming. In particular, the mean SST of the central Pacific is relatively high, and thus the latent heat flux is more sensitive to the change in wind speed (Yeh et al. 2014). Interestingly, there are significant positive wind speed anomalies near 135°W for the DP El Niño in Fig. 7b, possibly due to the easterly wind anomaly there (Fig. 4c). This

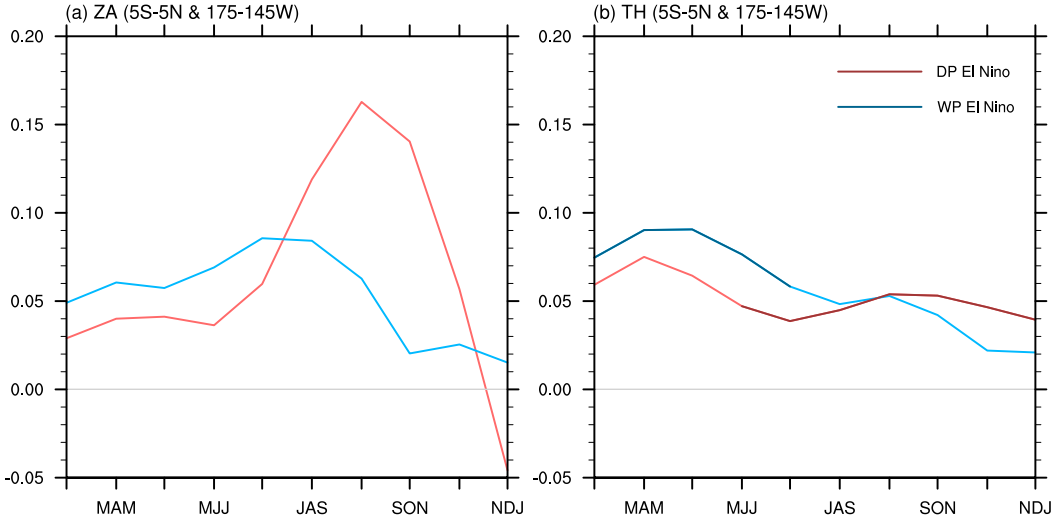

FIG. 6. Time series (month^{-1}) of the (a) normalized zonal advective feedback and (b) normalized thermocline feedback term in the central peak area. These are averaged by 5°S–5°N and 175°–145°W. The light-pink line indicates the DP El Niño, and the light-blue line indicates the WP El Niño. The dark lines indicate the 90% confidence level.

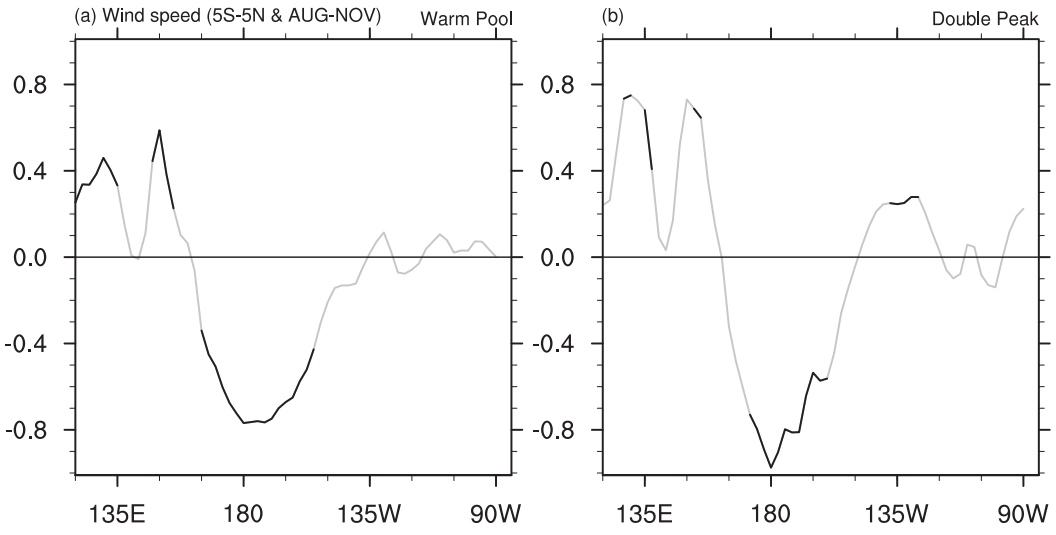

FIG. 7. Normalized anomalous wind speed ($m\,s^{-1}\,°C^{-1}$) in the development phase averaged by equator for (a) the WP El Niño and (b) the DP El Niño. Black lines indicate the 90% confidence level.

indicates enhanced evaporative cooling there, which likely plays a role in reducing the warm anomalies. The location of the reduced anomalies is similar to the location where the number of the SSTA peak is minimized, as shown in Fig. 2. This relationship should be examined in a future study. Based on Figs. 5a, 6, and 7, we conclude that the central peak of the DP El Niño develops by the zonal advective feedback and latent heat flux feedback, similar to the WP El Niño, although the timing of the evolutions differs.

c. *The eastern peak of the DP El Niño*

As shown in Fig. 4, the DP and WP El Niño show very similar central Pacific SSTA patterns, but quite distinct magnitudes in the eastern Pacific SSTA. For example, the eastern Pacific SSTA (120°–90°W) during NDJ is 0.55 and 0.95 K for the WP and DP El Niños, respectively. As shown in the temperature tendency budget (Fig. 5b), it is evident that the total advection term of the DP El Niño is about 2.5 times larger than that of the WP El Niño. That is why the eastern peak only happens in the DP El Niño. As expected, the thermocline feedback term is the dominant term in the eastern peak of the DP El Niño. The meridional term by the climatological current and anomalous temperature gradient is also large in the DP and WP El Niño, but this term indicates a meridional expansion of the equatorial SSTA as mentioned in section 3b. Therefore, the term that drives the development of the eastern peak is mainly the thermocline feedback term.

Figure 8 shows why the DP El Niño has stronger thermocline feedback in the eastern Pacific compared to the WP El Niño. The sea level anomalies in the DP El Niño are much larger than those in the WP El Niño (Figs. 8a,b). The higher sea level anomalies are related to the deeper thermocline depth anomalies, which means the anomalous vertical temperature gradients are large due to the warmer subsurface temperature anomalies; thus, the higher sea level anomalies in the eastern Pacific are linked in the strong positive thermocline feedback term. The positive sea level anomalies in the eastern Pacific are related to the equatorial westerly wind stress anomalies. The equatorial westerly wind stress anomalies in the central Pacific are much stronger in the DP El Niño than that in the WP El Niño (Figs. 8c,d), in spite of the similar pattern of anomalous zonal wind stress. Note that the central Pacific SSTA in the WP El Niño is even stronger than those in the DP El Niño, suggesting that other processes as well as the equatorial SSTA forcing contribute to the strong westerly wind stress anomalies of the DP El Niño. The precipitation anomalies also show distinct magnitudes between the WP and DP El Niños. As shown in Figs. 8e and 8f, the equatorial positive precipitation anomalies of the DP El Niño are stronger than those for the WP El Niño, which is partly due to the higher eastern Pacific SSTA. In addition to the equatorial precipitation, there are distinct differences in the Northern Hemisphere off-equator precipitation anomalies. That is, strong positive precipitation anomalies exist along the Pacific ITCZ in the DP El Niño events. These off-equatorial positive precipitation anomalies can also contribute to the strong westerly wind stress anomalies in the DP El Niño events.

To show the difference in the magnitudes of the key processes, the precipitation, zonal wind stress, and sea level anomalies are averaged in the regions 4°–8°N and 165°–135°W, 5°S–5°N and 170°E–160°W, and 5°S–5°N and 120°–90°W over August to November (Fig. 9). As shown in Fig. 9a, the ITCZ precipitation anomalies are significant in both cases, but the magnitude of the DP El Niño is about 2 times that of the WP El Niño. Also, the equatorial zonal wind stress anomaly of the DP El Niño is about 1.3 times and the sea level anomaly of the DP El Niño is about 1.5 times that for the WP El Niño.

From the equatorial Sverdrup balance (Jin 1997a; Jin and An 1999), the eastern Pacific sea level anomaly can be simply explained as follows:

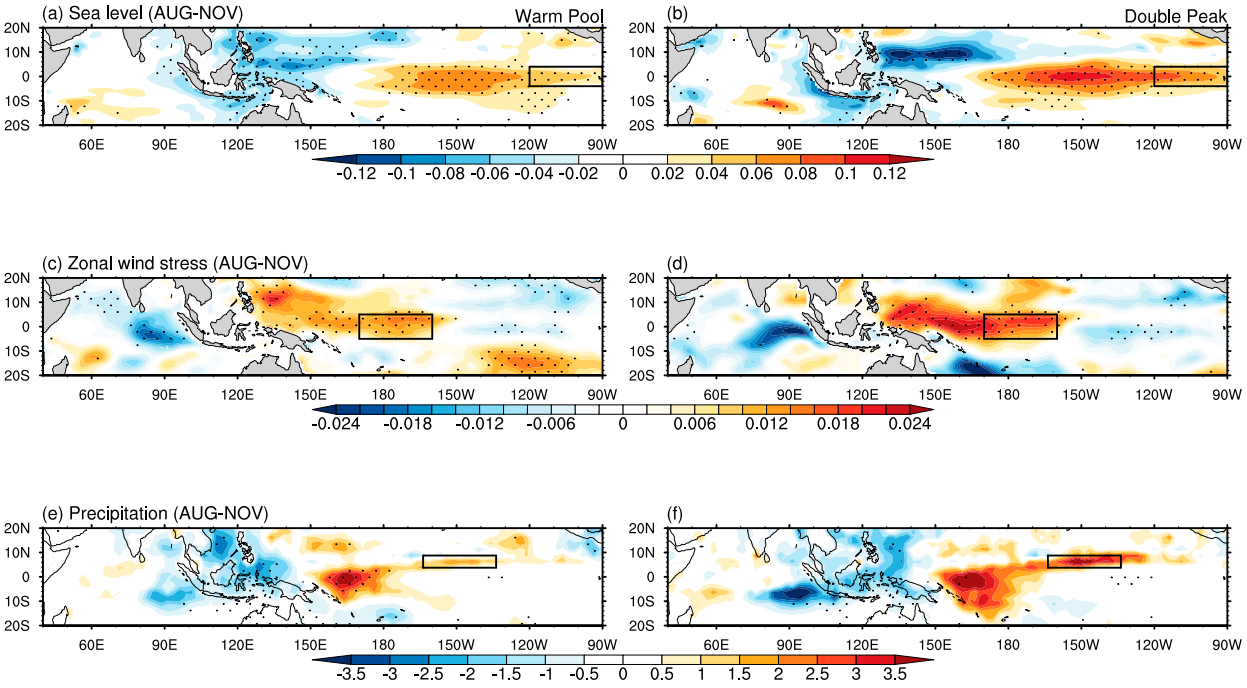

FIG. 8. Composite of the (a),(b) sea level anomalies (m °C^{-1}); (c),(d) zonal wind stress anomalies (N m^{-2} °C^{-1}); and (e),(f) precipitation anomalies (mm day^{-1} °C^{-1}) for the development period (all variables are normalized as in Fig. 3) for (left) the WP El Niño and (right) the DP El Niño. Stippling indicates regions where values are significant at the 90% confidence level. Black boxes represent the area where the difference appears.

$$g\int_0^x \frac{\partial h}{\partial x}dx \cong \frac{1}{\rho H}\int_0^x \tau_x\, dx \quad \text{and} \tag{1}$$

$$h(x) \cong h(0) + \frac{1}{\rho H g}\int_0^x \tau_x\, dx, \tag{2}$$

where x is the longitude (positive is eastward), h is the sea level anomalies averaged over the equator (5°S–5°N) and development period (August–November), τ_x is the x component of wind stress anomalies averaged over the equator and development period (N m^{-2}), g is the gravity (9.8 m s^{-2}), H(m) is the effective thermocline depth [which is determined by the root-mean-square difference between the sea level anomaly in the reanalysis data and the sea level anomaly obtained above in Eq. (2)], and ρ is the seawater density (1025 kg m^{-3}). Here, $h(x)$ is the sea level anomaly (m) at the particular longitude (we set this at 105°W, the center of the black box area in Fig. 8b) that can be calculated from Eq. (2); $h(0)$ is the sea level anomaly at the starting longitude (150°E), and the last term is

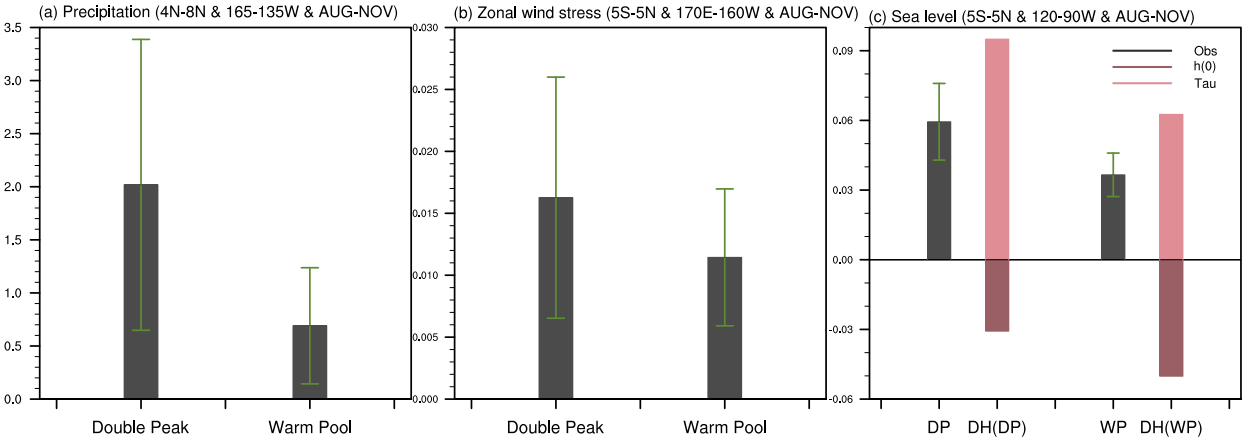

FIG. 9. Normalized indices of the black-boxed areas in Fig. 8 for (a) precipitation anomalies, (b) zonal wind stress anomalies, and (c) sea level anomalies. The light-pink bars indicate the integrated anomalous zonal wind stress terms, and dark-pink bars indicate the sea level at the starting longitude (150°E). Green error bars indicate the 90% confidence level. Units are the same as for Fig. 8.

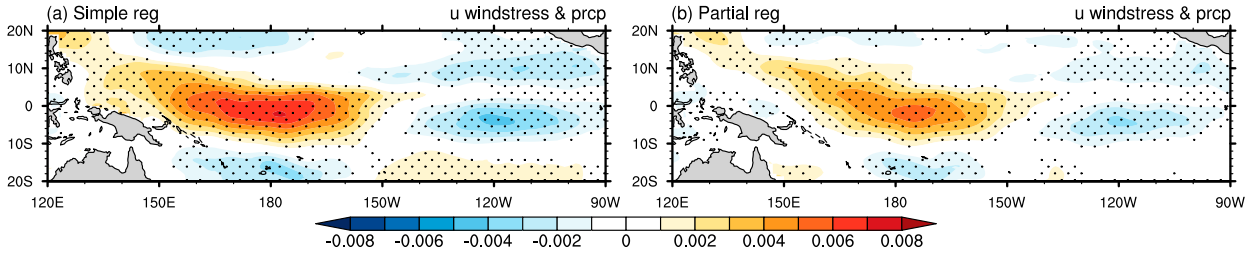

FIG. 10. Regression coefficients of (a) simple linear regression between the zonal wind stress anomalies and the anomalous ITCZ precipitation index (4°–8°N, 165°–135°W) and (b) partial linear regression after the effect of the anomalous precipitation index in the western-central Pacific (5°S–5°N, 150°E–180°) is linearly removed. Stippling indicates regions where values are significant at the 95% confidence level.

the zonal integrated x component of wind stress anomalies from the western Pacific to the eastern Pacific (150°E–105°W). Figure 9c shows each term of Eq. (2). As expected, the zonally integrated wind stress anomalies along the equator are much larger in the DP El Niño event, which contributes to the higher sea level anomalies in the eastern Pacific. These strong westerly wind stress anomalies along the equator can induce the downwelling Kelvin waves and propagate to the eastern Pacific. Thus, the DP El Niño has higher sea level anomalies in the eastern Pacific than the WP El Niño. Also, the sea level anomaly at the western boundary is more strongly negative in the WP El Niño. Therefore, the higher eastern Pacific sea level anomalies of the DP El Niño can be explained by the stronger equatorial zonal wind stress anomalies and weaker negative sea level anomalies at the western Pacific. When we compared the evolution of the sea level anomalies, the WP El Niño has a lower anomalous sea level from FMA than the DP El Niño (not shown). The weak negative sea level anomalies at the western boundary are related to the late development of the DP El Niño. The WP El Niño already shows significant SSTA in the central Pacific in early summer (Fig. 3b), which induces an equatorial westerly wind stress anomaly and off-equatorial cyclonic wind stress curl anomaly. The cyclonic curl excites upwelling Rossby waves, which propagate westward and are reflected as an upwelling Kelvin wave at the western boundary, contributing to the negative sea level anomalies in the eastern Pacific. However, since the DP El Niño has weaker SSTA and wind patterns in early summer due to the late development, the negative sea level anomalies are weaker than those in the WP El Niño. This means a weaker contribution of the reflected upwelling Kelvin waves and less cancelation for the contribution of the westerly induced downwelling Kelvin waves in the eastern Pacific, resulting in the stronger sea level. These differences can lead to different sea level responses in the eastern Pacific in late summer and autumn.

Therefore, we conclude that the higher sea level anomalies in the eastern Pacific result from the equatorial westerly wind stress anomalies and sea level anomalies in the western Pacific. That is, the DP El Niño has a less low sea level anomaly in the western Pacific and stronger wind stress anomaly along the equator, which can induce the higher sea level anomaly in the eastern Pacific. Finally, the eastern peak of the DP El Niño can be generated by the advection of the anomalous warm water in the subsurface advected by the mean upwelling (i.e., thermocline feedback term).

A key question is, Why does the DP El Niño have the stronger equatorial westerly wind stress anomaly? This can be related to stronger precipitation anomalies in the western-central Pacific as shown in Figs. 8e and 8f. In addition, there are distinctive differences in the precipitation anomalies along the Pacific ITCZ. This stronger precipitation anomaly may contribute to the anomalous equatorial westerly wind stress. To examine the effect of the ITCZ precipitation anomaly, Fig. 10a shows the simple linear regression of the zonal wind stress anomalies against the anomalous ITCZ precipitation index, defined by averaging the precipitation anomalies over 4°–8°N and 165°–135°W. It is clear that the anomalous ITCZ precipitation is related to the westerly wind stress anomalies in the western-central Pacific and weaker easterlies in the eastern Pacific. However, this linear relationship can result from other factors correlated to the ITCZ precipitation anomaly, such as the western-central Pacific precipitation anomaly (5°S–5°N, 150°E–180°). In fact, the correlation between the ITCZ precipitation anomaly and the western-central Pacific precipitation anomaly is about 0.65. Thus, we calculated a partial regression with respect to the ITCZ precipitation anomaly after linearly removing the effect of the western-central Pacific precipitation. As shown in Fig. 10b, even with this removal there are still westerlies in the western-central Pacific. Easterly wind stress anomalies are evident in the Northern Hemisphere subtropical region and Southern Hemisphere off-equatorial eastern Pacific. This wind pattern is quite similar to the idealized Gill-type response to off-equatorial heating (Gill 1980). The Rossby wave response to the off-equatorial heating can explain the easterlies to the east of the heating.

To further quantify what causes the different equatorial zonal wind patterns between the DP and WP El Niño, we conducted LBM experiments. Figure 11 shows the effect of precipitation anomalies on the low-level wind anomalies (850 hPa). With prescribed precipitation anomalies over the tropics (10°S–10°N, for all longitudes), the LBM model simulates anomalous westerlies in the DP El Niño over the western-central Pacific (5°S–5°N, 160°E–160°W) that are about 2.6 times stronger (Figs. 11a, 11b, and 11i). In fact, the observed westerly wind anomalies of the DP El Niño are also 1.4 times those of the WP El Niño over the western-central Pacific (not

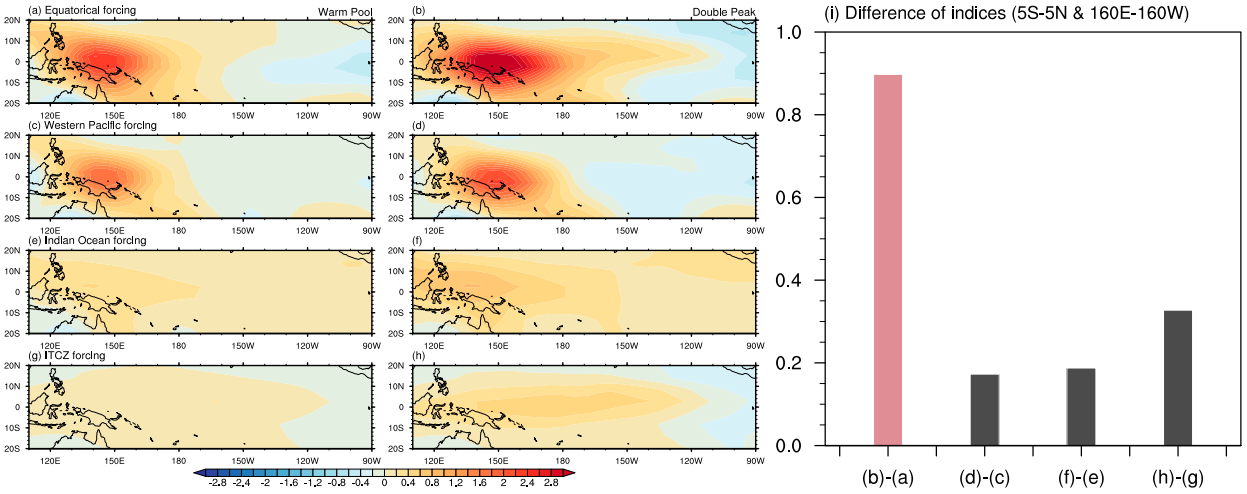

FIG. 11. The 850-hPa zonal wind anomalies (m s^{-1}) from the LBM. We experiment with different forcing areas. The forcing areas are (a),(b) the whole longitude; (c),(d) the western Pacific area (110°E–180°); and (e),(f) the Indian Ocean area (60°–110°E), and in common 10°S–10°N. (g),(h) Forced only by the ITCZ area (4°–10°N, 180°–120°W). Forcing is shown for (left) the WP El Niño and (center) the DP El Niño. (i) The differences in the anomalous wind for 5°S–5°N and 160°E–160°W.

shown). This suggests that the anomalous tropical precipitation is the dominant driver of the wind anomalies between the WP and DP El Niño.

To understand the locations where precipitation anomaly is more important for the difference of the wind anomaly, we carry out additional experiments by only prescribing precipitation anomaly for particular regions. Figures 11c–h show the results for the forcing region in the western Pacific (10°S–10°N, 110°E–180°), the Indian Ocean and Maritime Continent region (10°S–10°N, 60°–110°E), and for the ITCZ (4°–10°N, 180°–120°W). The western Pacific precipitation explains approximately 19.2% of the wind difference (Figs. 11c,d,i) between the anomalous zonal wind response in Figs. 11a and 11b. Also, the Indian Ocean precipitation explains approximately 20.9% of the difference (Figs. 11e,f,i). Last, if we only prescribe precipitation in the ITCZ line, there is a relatively large difference in the western-central Pacific in Figs. 11g and 11h. To quantify the contribution of the ITCZ in Figs. 11g and 11h, it can explain about 36.5% of the wind difference in Figs. 11a and 11b (Fig. 11i). Thus, the difference of the wind response in the western-central Pacific between the WP and DP El Niño is affected by the ITCZ precipitation of about 36.5%. In spite of a relatively small area of ITCZ precipitation, these results suggest that the Pacific ITCZ precipitation is critical for the stronger westerly anomalies, which lead to the development of the DP El Niño.

4. Summary and discussion

We have shown here that the DP El Niño, first identified by Graham et al. (2017), exists not only in coupled model simulations but also in the observations. Distinct from the CT El Niños, the WP and DP El Niño show similar patterns of anomalous precipitation and zonal wind stress, in spite of the clear differences in the eastern Pacific SSTA. As a result, the DP SST structure is a new pattern in terms of the zonal diversity of ENSO. Each center of DP El Niño is mainly caused by zonal advective and thermocline feedback terms, respectively, which are fundamentally originated from the same equatorial air–sea interaction such as the increased precipitation and resultant zonal wind stress. However, the evolving processes of central and eastern peaks are different. First, we found that the mechanism of the central peak of the DP El Niño is consistent with that of the WP El Niño. That is, the zonal advective feedback term by the anomalous eastward currents and the mean temperature gradient, and the latent heat flux due to the reduced wind speed anomaly, are also important for the DP El Niño.

Second, the main difference between the WP and DP El Niños is found in the eastern equatorial Pacific. The DP El Niños have a deeper (higher) thermocline (sea level) in the eastern Pacific than that of the WP El Niño, which leads to the stronger thermocline feedback term. The higher eastern Pacific anomalous sea level is related to the late development of the DP El Niño. In addition, the stronger westerly wind stress anomalies in the western-central Pacific also contribute to the stronger sea level anomalies responses. We find that the strong westerly wind anomalies may be related to a peculiar precipitation anomaly along the Pacific ITCZ (i.e., between 4° and 8°N and 165° and 135°W). The positive precipitation anomaly along the Pacific ITCZ can enhance the equatorial westerlies as a result of the Gill-type response to off-equatorial heating. These westerly wind stress anomalies along the equator can excite downwelling Kelvin waves that propagate eastward and induce higher sea level anomalies in the eastern Pacific.

This distinct anomalous precipitation pattern of the DP El Niño implies why the observed DP El Niño, clearly detected and identified in the observations here for the first time, is important for climate studies. Although the anomalous precipitation patterns are similar in the equatorial western and

central Pacific between the WP and DP El Niño, the distinct off-equatorial precipitation anomaly may suggest different global impacts. Recently, several studies pointed out that off-equatorial SSTA and precipitation anomaly are very important for ENSO teleconnections (Jin et al. 2013; Son et al. 2016; Kim and Kug 2019). Therefore, the distinct impacts of the DP El Niño should be further investigated.

Although our study only focused on the dynamic mechanism of the DP El Niño during the development period, one of the distinctive features of the DP El Niño is the rapid development and decay. In particular, the decay is extremely fast, such that the positive SSTA in the eastern equatorial Pacific abruptly decays in late winter and early spring. This might be related to a stronger discharge of the equatorial heat content (Jin 1997a). The DP El Niño has the stronger cyclonic wind stress curl anomalies in the off-equatorial region in the central Pacific because of the stronger equatorial westerly wind stress anomalies from the development phase to the mature phase (Figs. 4 and 7). This westerly wind stress anomaly can reinforce the discharge process, which can lead to the fast decay. However, more detailed analysis on the decay process should be investigated in a future study.

In this study, we examined El Niño events in the last 40 years and detected three DP El Niño events in the historical SSTA observations. Interestingly, the three DP El Niño events are observed only in the past 20 years (2002/03, 2006/07, and 2018/19), which suggests that favorable conditions have been more prevalent in recent decades for the occurrence of DP El Niño event. It is conceivable that the recent La Niña–like trend is responsible for the more frequent emergence of the DP El Niño in the past 20 years. The La Niña–like SST background accompanies relatively dry conditions in the central and eastern Pacific, which can suppress the anomalous precipitation response to a given eastern Pacific SSTA forcing (Watanabe et al. 2012; Ham and Kug 2012; Jang et al. 2013; Ham and Kug 2015). Instead, the precipitation anomalies tend to shift to the western Pacific and off the equator where the convective instability is relatively stronger (Watanabe et al. 2011; Kim et al. 2011). As we discussed in Fig. 8, the DP El Niño shows distinctively stronger precipitation anomalies along the Pacific ITCZ as well as stronger western-central Pacific precipitation anomalies in spite of the slightly weaker central Pacific SSTA. These features are consistent with the conditions associated with the La Niña–like trend. In addition, this argument is consistent with the finding of Graham et al. (2017) from their analysis of coupled climate model simulations of ENSO. They argued that the cold-tongue bias in the coupled models leads to a preference for DP El Niño occurrence due to the westward shifted mean temperature gradient and anomalous eastward currents. In terms of the drier and cooler equatorial zone, the cold-tongue bias and the La Niña–like trend are consistent. However, some studies argued that the La Niña–like trend ended in around 2016 (Meehl et al. 2016; Su et al. 2017; Hu and Fedorov 2017; Hu et al. 2020). Based on these studies, the 2018/19 happened under a different background state. Therefore, we need to also consider a possibility for other mechanisms. This will require a further research for the future DP El Niño cases.

Although we clearly showed the existence of the DP El Niño in the observational data, our study has several caveats. First of all, our study has a clear limitation due to the small sample size. Since we separate El Niño events into three groups in this study for 40 years, it is unavoidable that each group has a small number of samples. Therefore, interpretation of the statistical analysis, presented here, is bound to be limited. For example, the role of the ITCZ precipitation is commonly robust for the three DP El Niño events in our analysis. However, it will be also possible that the other processes can enhance the equatorial westerlies, and lead to the development of DP SST structure. Therefore, a more general conclusion for the DP El Niño development should be followed by a further study with a more accumulated observational analysis.

Second, the selection of DP El Niño depends on the criteria of the SST anomaly. We used here the criteria of one standard deviation to pick up the warm point, but a slight change of this criteria brings about different groupings. For example, the 2014 warm event clearly showed the DP structure (see Fig. 1 of McPhaden 2015), but it was not selected due to the one standard deviation criteria. If we change the criteria to 0.7 standard deviations, 1987/88, 2003/04, and 2014/15 years are additionally selected as the DP El Niño year. Some WP El Niño cases can be moved to the DP El Niño case depending on the criteria. Importantly, however, we checked that major characteristics such as the late development (except for the 1987/88 El Niño because it happened consecutively with 1986/87 El Niño) and enhanced ITCZ precipitation anomalies are not sensitive to how to define DP El Niño, though detailed patterns are slightly different (see Figs. S1 and S2 in the online supplemental material). This supports our key arguments that the El Niño events having DP structure exist in the observation, and a particular physical process provides a favorable condition for the occurrence of DP SST pattern.

Third, the selection of DP El Niño can be data dependent as well as the criteria. We checked the other observed SST dataset (e.g., OISST, HadISST, Kaplan, TropFlux, TOGA-TAO, and GODAS), and analyzed interdata consistency. We found that most SST data show consistent DP structure for the 2002/03, 2006/07, and 2018/19 El Niño cases (see Fig. S3 in the online supplemental material). Especially, every dataset shows a clear DP structure for the 06/07 El Niño event. However, it is also evident that there are some interdata inconsistencies. The inconsistencies are relatively large for 2002/03 El Niño. In particular, the HadISST data show the DP structure only for the 2006/07 case. This inconsistency may be related to relatively large uncertainty in the eastern Pacific, where observations are sparce and variability is large (Huang et al. 2020). Though the data uncertainty prevents from drawing a concrete conclusion for detailed processes of DP El Niño, it is certain that every data exhibit the pattern of the DP SST structure (i.e., 2006/07 El Niño), supporting the existence of observed DP El Niño. Along this line, a more detailed analysis of the influence of the dataset on the occurrence of the DP El Niño event should be further examined.

Acknowledgments. This study is supported by the National Research Foundation of Korea (NRF-2018R1A5A1024958).

Author Holbrook acknowledges funding received from the Australian Research Council Centre of Excellence for Climate Extremes (CE170100023) and the National Environmental Science Programme Earth Systems and Climate Change Hub.

Data availability statement. The ERSST, version 5 (v5), monthly reanalysis data were downloaded from https://www.esrl.noaa.gov/psd/data/gridded/data.noaa.ersst.v5.html. The NCEP–NCAR reanalysis, version 1 (v1), data are from https://www.esrl.noaa.gov/psd/data/gridded/data.ncep.reanalysis.pressure.html. The GODAS data were downloaded from https://psl.noaa.gov/data/gridded/data.godas.html.

REFERENCES

Ashok, K., S. K. Behera, S. A. Rao, H. Weng, and T. Yamagata, 2007: El Niño Modoki and its possible teleconnection. *J. Geophys. Res.*, **112**, C11007, https://doi.org/10.1029/2006JC003798.

Behringer, D., and Y. Xue, 2004: Evaluation of the global ocean data assimilation system at NCEP: The Pacific Ocean. *Eighth Symp. on Integrated Observing and Assimilation System for Atmosphere, Ocean, and Land Surface*, Seattle, WA, Amer. Meteor. Soc., 2.3, https://ams.confex.com/ams/pdfpapers/70720.pdf.

Bjerknes, J., 1969: Atmospheric teleconnections from the equatorial Pacific. *Mon. Wea. Rev.*, **97**, 163–172, https://doi.org/10.1175/1520-0493(1969)097<0163:ATFTEP>2.3.CO;2.

Brown, J. N., C. Langlais, and C. Maes, 2013: Zonal structure and variability of the western Pacific dynamic warm pool edge in CMIP5. *Climate Dyn.*, **42**, 3061–3076, https://doi.org/10.1007/s00382-013-1931-5.

Cai, W., and Coauthors, 2019: Pantropical climate interactions. *Science*, **363**, eaav4236, https://doi.org/10.1126/science.aav4236.

Cane, M. A., and S. E. Zebiak, 1985: A theory for El Niño and the Southern Oscillation. *Science*, **228**, 1085–1087, https://doi.org/10.1126/science.228.4703.1085.

Capotondi, A., and Coauthors, 2015: Understanding ENSO diversity. *Bull. Amer. Meteor. Soc.*, **96**, 921–938, https://doi.org/10.1175/BAMS-D-13-00117.1.

——, P. D. Sardeshmukh, E. D. Lorenzo, A. C. Subramanian, and A. J. Miller, 2019: Predictability of US West Coast ocean temperatures is not solely due to ENSO. *Sci. Rep.*, **9**, 10993, https://doi.org/10.1038/s41598-019-47400-4.

Clarke, A. J., J. Wang, and S. V. Gorder, 2000: A simple warm-pool displacement ENSO model. *J. Phys. Oceanogr.*, **30**, 1679–1691, https://doi.org/10.1175/1520-0485(2000)030<1679:ASWPDE>2.0.CO;2.

Gill, A. E., 1980: Some simple solutions for heat-induced tropical circulation. *Quart. J. Roy. Meteor. Soc.*, **106**, 447–462, https://doi.org/10.1002/qj.49710644905.

Graham, F. S., A. T. Wittenberg, J. N. Brown, S. J. Marsland, and N. J. Holbrook, 2017: Understanding the double peaked El Niño in coupled GCMs. *Climate Dyn.*, **48**, 2045–2063, https://doi.org/10.1007/s00382-016-3189-1.

Ham, Y.-G., and J.-S. Kug, 2012: How well do current climate models simulate two types of El Niño? *Climate Dyn.*, **39**, 383–398, https://doi.org/10.1007/s00382-011-1157-3.

——, and ——, 2015: Improvement of ENSO simulation based on intermodel diversity. *J. Climate*, **28**, 998–1015, https://doi.org/10.1175/JCLI-D-14-00376.1.

Hirst, A. C., 1986: Unstable and damped equatorial modes in simple coupled ocean–atmosphere models. *J. Atmos. Sci.*, **43**, 606–632, https://doi.org/10.1175/1520-0469(1986)043<0606:UADEMI>2.0.CO;2.

Hoerling, M. P., A. Kumar, and M. Zhong, 1997: El Niño, La Niña, and the nonlinearity of their teleconnections. *J. Climate*, **10**, 1769–1786, https://doi.org/10.1175/1520-0442(1997)010<1769:ENOLNA>2.0.CO;2.

Hu, S., and A. V. Fedorov, 2017: The extreme El Niño of 2015–2016 and the end of global warming hiatus. *Geophys. Res. Lett.*, **44**, 3816–3824, https://doi.org/10.1002/2017GL072908.

Hu, Z.-Z., A. Kumar, B. Huang, J. Zhu, M. L'Heureux, M. J. McPhaden, and J.-Y. Yu, 2020: The interdecadal shift of ENSO properties in 1999/2000: A review. *J. Climate*, **33**, 4441–4462, https://doi.org/10.1175/JCLI-D-19-0316.1.

Huang, B., Y. Xue, D. Zhang, A. Kumar, and M. J. McPhaden, 2010: The NCEP GODAS ocean analysis of the tropical Pacific mixed layer heat budget on seasonal to interannual time scales. *J. Climate*, **23**, 4901–4925, https://doi.org/10.1175/2010JCLI3373.1.

——, and Coauthors, 2017: Extended Reconstructed Sea Surface Temperature, version 5 (ERSSTv5): Upgrades, validations, and intercomparisons. *J. Climate*, **30**, 8179–8205, https://doi.org/10.1175/JCLI-D-16-0836.1.

——, and Coauthors, 2020: Uncertainty estimates for sea surface temperature and land surface air temperature in NOAAGlobalTemp version 5 Uncertainty estimates for sea surface temperature and land surface air temperature in NOAAGlobalTemp version 5. *J. Climate*, **33**, 1351–1379, https://doi.org/10.1175/JCLI-D-19-0395.1.

Jang, Y.-S., D. Kim, Y.-H. Kim, D.-H. Kim, M. Watanabe, F.-F. Jin, and J.-S. Kug, 2013: Simulation of two types of El Niño from different convective parameters. *Asia-Pac. J. Atmos. Sci.*, **49**, 193–199, https://doi.org/10.1007/s13143-013-0020-3.

Jin, C.-S., C.-H. Ho, J.-H. Kim, D.-K. Lee, D.-H. Cha, and S.-W. Yeh, 2013: Critical role of northern off-equatorial sea surface temperature forcing associated with central Pacific El Niño in more frequent tropical cyclone movements toward East Asia. *J. Climate*, **26**, 2534–2545, https://doi.org/10.1175/JCLI-D-12-00287.1.

Jin, F.-F., 1997a: An equatorial ocean recharge paradigm for ENSO. Part II: A stripped-down coupled model. *J. Atmos. Sci.*, **54**, 830–847, https://doi.org/10.1175/1520-0469(1997)054<0830:AEORPF>2.0.CO;2.

——, 1997b: An equatorial ocean recharge paradigm for ENSO. Part I: Conceptual model. *J. Atmos. Sci.*, **54**, 811–829, https://doi.org/10.1175/1520-0469(1997)054<0811:AEORPF>2.0.CO;2.

——, and S.-I. An, 1999: Thermocline and zonal advective feedbacks within the equatorial ocean recharge oscillator model for ENSO. *Geophys. Res. Lett.*, **26**, 2989–2992, https://doi.org/10.1029/1999GL002297.

Kalnay, E., and Coauthors, 1996: The NCEP/NCAR 40-Year Reanalysis Project. *Bull. Amer. Meteor. Soc.*, **77**, 437–471, https://doi.org/10.1175/1520-0477(1996)077<0437:TNYRP>2.0.CO;2.

Kang, I.-S., S.-I. An, and F.-F. Jin, 2001: A systematic approximation of the SST anomaly equation for ENSO. *J. Meteor. Soc. Japan*, **79**, 1–10, https://doi.org/10.2151/jmsj.79.1.

Kao, H.-Y., and J.-Y. Yu, 2009: Contrasting eastern-Pacific and central-Pacific types of ENSO. *J. Climate*, **22**, 615–632, https://doi.org/10.1175/2008JCLI2309.1.

Kim, D., Y.-S. Jang, D.-H. Kim, Y.-H. Kim, M. Watanabe, F.-F. Jin, and J.-S. Kug, 2011: El Niño–Southern Oscillation sensitivity to cumulus entrainment in a coupled general circulation model. *J. Geophys. Res.*, **116**, D22112, https://doi.org/10.1029/2011jd016526.

Kim, J.-S., and J.-S. Kug, 2019: Role of off-equatorial SST in El Niño teleconnection to East Asia during El Niño decaying spring. *Climate Dyn.*, **52**, 7293–7308, https://doi.org/10.1007/s00382-016-3473-0.

Kim, S., H.-Y. Son, and J.-S. Kug, 2018: Relative roles of equatorial central Pacific and western North Pacific precipitation anomalies in ENSO teleconnection over the North Pacific. *Climate Dyn.*, **51**, 4345–4355, https://doi.org/10.1007/s00382-017-3779-6.

Kug, J.-S., F.-F. Jin, and S.-I. An, 2009: Two types of El Niño events: Cold tongue El Niño and warm pool El Niño. *J. Climate*, **22**, 1499–1515, https://doi.org/10.1175/2008JCLI2624.1.

——, M.-S. Ahn, M.-K. Sung, S.-W. Yeh, H.-S. Min, and Y.-H. Kim, 2010a: Statistical relationship between two types of El Niño events and climate variation over the Korean Peninsula. *Asia-Pac. J. Atmos. Sci.*, **46**, 467–474, https://doi.org/10.1007/s13143-010-0027-y.

——, J. Choi, S.-I. An, F.-F. Jin, and A. T. Wittenberg, 2010b: Warm pool and cold tongue El Niño events as simulated by the GFDL 2.1 coupled GCM. *J. Climate*, **23**, 1226–1239, https://doi.org/10.1175/2009JCLI3293.1.

Larkin, N. K., and D. E. Harrison, 2005a: Global seasonal temperature and precipitation anomalies during El Niño autumn and winter. *Geophys. Res. Lett.*, **32**, L16705, https://doi.org/10.1029/2005GL022860.

——, and ——, 2005b: On the definition of El Niño and associated seasonal average U.S. weather anomalies. *Geophys. Res. Lett.*, **32**, L13705, https://doi.org/10.1029/2005GL022738.

McPhaden, M. J., 2015: Playing hide and seek with El Niño. *Nat. Climate Change*, **5**, 791–795, https://doi.org/10.1038/nclimate2775.

Meehl, G. A., A. Hu, B. D. Santer, and S.-P. Xie, 2016: Contribution of the interdecadal Pacific oscillation to twentieth-century global surface temperature trends. *Nat. Climate Change*, **6**, 1005–1008, https://doi.org/10.1038/nclimate3107.

Philander, S. G. H., T. Yamagata, and R. C. Pacanowski, 1984: Unstable air–sea interactions in the tropics. *J. Atmos. Sci.*, **41**, 604–613, https://doi.org/10.1175/1520-0469(1984)041<0604:UASIIT>2.0.CO;2.

Picaut, J., M. Ioualalen, C. Menkes, T. Delcroix, and M. J. McPhaden, 1996: Mechanism of the zonal displacements of the Pacific warm pool: Implications for ENSO. *Science*, **274**, 1486–1489, https://doi.org/10.1126/science.274.5292.1486.

——, F. Masia, and Y. du Penhoat, 1997: An advective-reflective conceptual model for the oscillatory nature of the ENSO. *Science*, **277**, 663–666, https://doi.org/10.1126/science.277.5326.663.

Rashid, H. A., and A. C. Hirst, 2015: Investigating the mechanisms of seasonal ENSO phase locking bias in the ACCESS coupled model. *Climate Dyn.*, **46**, 1075–1090, https://doi.org/10.1007/s00382-015-2633-y.

Rasmusson, E. M., and T. H. Carpenter, 1982: Variations in tropical sea surface temperature and surface wind fields associated with the Southern Oscillation/El Niño. *Mon. Wea. Rev.*, **110**, 354–384, https://doi.org/10.1175/1520-0493(1982)110<0354:VITSST>2.0.CO;2.

Shi, J., A. V. Fedorov, and S. Hu, 2019: North Pacific temperature and precipitation response to El Niño-like equatorial heating: Sensitivity to forcing location. *Climate Dyn.*, **53**, 2731–2741, https://doi.org/10.1007/s00382-019-04655-x.

Son, H.-Y., J.-Y. Park, J.-S. Kug, J. Yoo, and C.-H. Kim, 2014: Winter precipitation variability over Korean Peninsula associated with ENSO. *Climate Dyn.*, **42**, 3171–3186, https://doi.org/10.1007/s00382-013-2008-1.

——, ——, and ——, 2016: Precipitation variability in September over the Korean Peninsula during ENSO developing phase. *Climate Dyn.*, **46**, 3419–3430, https://doi.org/10.1007/s00382-015-2776-x.

Su, J., R. Zhang, T. Li, X. Rong, J.-S. Kug, and C.-C. Hong, 2010: Causes of the El Niño and La Niña amplitude asymmetry in the equatorial eastern Pacific. *J. Climate*, **23**, 605–617, https://doi.org/10.1175/2009JCLI2894.1.

——, ——, and H. Wang, 2017: Consecutive record-breaking high temperatures marked the handover from hiatus to accelerated warming. *Sci. Rep.*, **7**, 43735, https://doi.org/10.1038/srep43735.

Timmermann, A., and Coauthors, 2018: El Niño–Southern Oscillation complexity. *Nature*, **559**, 535–545, https://doi.org/10.1038/s41586-018-0252-6.

Trenberth, K. E., G. W. Branstator, D. Karoly, A. Kumar, N.-C. Lau, and C. Ropelewski, 1998: Progress during TOGA in understanding and modeling global teleconnections associated with tropical sea surface temperatures. *J. Geophys. Res.*, **103**, 14 291–14 324, https://doi.org/10.1029/97JC01444.

Wang, C., and R. H. Weisberg, 1994: On the "slow mode" mechanism in ENSO-related coupled ocean–atmosphere models. *J. Climate*, **7**, 1657–1667, https://doi.org/10.1175/1520-0442(1994)007<1657:OTMMIE>2.0.CO;2.

Watanabe, M., and M. Kimoto, 2000: Atmosphere-ocean thermal coupling in the North Atlantic: A positive feedback. *Quart. J. Roy. Meteor. Soc.*, **126**, 3343–3369, https://doi.org/10.1002/qj.49712657017.

——, M. Chikira, Y. Imada, and M. Kimoto, 2011: Convective control of ENSO simulated in MIROC. *J. Climate*, **24**, 543–562, https://doi.org/10.1175/2010JCLI3878.1.

——, J. Kug, F. Jin, M. Collins, M. Ohba, and A. T. Wittenberg, 2012: Uncertainty in the ENSO amplitude change from the past to the future. *Geophys. Res. Lett.*, **39**, L20703, https://doi.org/10.1029/2012GL053305.

Wyrtki, K., 1975: El Niño—The dynamic response of the equatorial Pacific Ocean to atmospheric forcing. *J. Phys. Oceanogr.*, **5**, 572–584, https://doi.org/10.1175/1520-0485(1975)005<0572:ENTDRO>2.0.CO;2.

Xie, P., and P. A. Arkin, 1997: Global precipitation: A 17-year monthly analysis based on gauge observations, satellite estimates, and numerical model outputs. *Bull. Amer. Meteor. Soc.*, **78**, 2539–2558, https://doi.org/10.1175/1520-0477(1997)078<2539:GPAYMA>2.0.CO;2.

Yeh, S.-W., J.-S. Kug, and S.-I. An, 2014: Recent progress on two types of El Niño: Observations, dynamics, and future changes. *Asia-Pac. J. Atmos. Sci.*, **50**, 69–81, https://doi.org/10.1007/s13143-014-0028-3.